DOI: 10.1002/ejic.201000374

# Water-Soluble Ultra-Small Manganese Oxide Surface Doped Gadolinium Oxide ($Gd_2O_3$@MnO) Nanoparticles for MRI Contrast Agent

**Eun Sook Choi,[a] Ja Young Park,[a] Myung Ju Baek,[b] Wenlong Xu,[a] Krishna Kattel,[a] Joo Hyun Kim,[c] Jae Jun Lee,[c] Yongmin Chang,*[c] Tae Jeong Kim,[d] Ji Eun Bae,[e] Kwon Seok Chae,[e] Kyung Jin Suh,[f] and Gang Ho Lee*[a]**

**Keywords:** Colloids / Imaging agents / Nanoparticles / Nanotechnology

We have developed ultra-small gadolinium oxide ($Gd_2O_3$) nanoparticles, which are surface-doped with manganese oxide (MnO) (abbreviated as $Gd_2O_3$@MnO). The surface-doped nanoparticles ranged from 1 to 2 nm in diameter. They were further coated with hydrophilic biocompatible lactobionic acid. In-vitro tests of the sample solution indicated clear dose-dependent contrast enhancements in both $T_1$ and $T_2$ map images, showing that the nanoparticles may be used as both $T_1$ and $T_2$ MRI contrast agents. Their performance as a $T_1$ MRI contrast agent was proved in vivo through $T_1$ MR images of a mouse.

## Introduction

The design of a new magnetic resonance imaging (MRI) contrast agent is a great challenge. Nanoparticle MRI contrast agents can provide us with a very high contrasting power through their enhanced relaxivities.[1,2] This capability of nanoparticles will allow us to acquire high-resolution MR images and detect diseases more easily.

So far, only the dextran-coated superparamagnetic iron oxides (SPIOs) have been developed as nanoparticle contrast agents and are now clinically used as negative $T_2$ contrast agents.[3–6] They possess a very high transverse relaxivity ($r_2$) of water protons of 100–200 $s^{-1}$ $mM^{-1}$. However, they are only liver-specific due to their large particle diameters ($> 10$ nm). Recently, paramagnetic manganese oxide[7] and gadolinium oxide nanoparticles[8–15] have drawn attention to themselves, because they may be used as highly sensitive positive $T_1$ MRI contrast agents through their high longitudinal relaxivities ($r_1$).

Among paramagnetic nanoparticle contrast agents, gadolinium-based nanoparticles are important, because they can have very high $r_1$ values, showing a very high positive contrasting ability. To date, $Gd_2O_3$,[8–15] $GdPO_4$,[16] $GdF_3$,[17] $Gd(BDC)_{1.5}\cdot(H_2O)_2$ (BDC = 1,4-benzenedicarboxylate),[18] $Gd_2O(CO_3)_2\cdot H_2O$,[19] and Gd-doped CdSe nanoparticles[20] have been studied. The primary reason for their high $r_1$ values is that $Gd^{III}$ possesses the largest spin magnetic moment ($S = 7/2$) in the Periodic Table because it consists of seven unpaired electrons ($4f^7$). These $S$-state electrons can efficiently induce longitudinal relaxation of water protons. It is worth noting that $S$-state electrons have a slow electron spin relaxation, which can easily interact with the longitudinal relaxation of water protons, whereas electrons with an orbital angular momentum have a rapid electron spin relaxation which is not good for the longitudinal relaxation of water protons.[21,22]

We have shown previously that the $r_1$ value of ultra-small $Gd_2O_3$ nanoparticles is at a maximum when the particle diameter is around 1–2.5 nm,[15] which differs from SPIOs with large particle diameters (the $r_2$ value of SPIOs increases with increasing particle diameter).[3–6] This ultra-small particle diameter is an important benefit for biological applications because ultra-small nanoparticles can be more easily excreted into the bladder than the conventional large nanoparticles.[13] This capability of ultra-small nanoparticles gives them the potential to be powerful MRI contrast agents for both non-specific and target-specific applications.

[a] Department of Chemistry, College of Natural Sciences, Kyungpook National University, Taegu 702-701, South Korea
Fax: +82-53-950-6330
E-mail: ghlee@mail.knu.ac.kr
[b] Department of Nanoscience and Nanotechnology, College of Natural Sciences, Kyungpook National University, Taegu 702-701, South Korea
[c] Department of Molecular Medicine and Medical & Biological Engineering, School of Medicine, Kyungpook National University and Hospital, Taegu 702-701, South Korea
E-mail: ychang@knu.ac.kr
[d] Department of Applied Chemistry, College of Engineering, Kyungpook National University, Taegu 702-701, South Korea
[e] Department of Biology Education, Teachers' College, Kyungpook National University, Taegu 702-701, South Korea
[f] Department of Radiology, College of Medicine, Dongguk University, Gyungju 780-714, South Korea

   

In this work we designed the $Gd_2O_3$@MnO nanoparticles by first synthesizing ultra-small $Gd_2O_3$ nanoparticles and then subsequently coating (or doping) them with MnO. They were further coated with lactobionic acid for biocompatibility and water solubility. The doping is different from the core-shell structure in terms of thickness (or concentration) of the shell. Both $r_1$ and $r_2$ will be largely determined by the shell in the case of the core-shell structure, because the shell will mostly contribute to the induction of water proton relaxation. Both the core and doping materials will, however, contribute to induction of water proton relaxations in the case of doping, because the core material is either very near or exposed to the surface. Therefore, doping will allow us to obtain maximal $r_1$ and $r_2$ values, because they will be determined by the material with a higher relaxivity. This doping can also reduce the toxicity of $Gd^{III}$ somewhat, because $Mn^{II}$ is nearly nontoxic.[23] Thus, ultra-small $Gd_2O_3$ nanoparticles can be doubly protected by both MnO and biocompatible lactobionic acid. We performed an in-vitro test of the sample solution by obtaining $T_1$ and $T_2$ map images. We observed that the sample solution clearly enhanced both $T_1$ and $T_2$ contrasts with an increasing dose. We measured their performance as $T_1$ MRI contrast agents by taking in-vivo $T_1$ MR images of a mouse.

## Results and Discussion

### 1. Particle Diameter

Figure 1a shows a high-voltage electron-microscope (HVEM) image of the lactobionic acid coated ultra-small $Gd_2O_3$@MnO nanoparticles. Particle diameters of the ultra-small $Gd_2O_3$@MnO nanoparticles are nearly monodisperse and estimated to be 1–2 nm. Figure 1b shows a scanning-tunneling electron-microscope (STEM) image, showing particle diameters of 2–3 nm. The difference between HVEM and STEM micrographs roughly corresponds to the surface coating by lactobionic acid (thickness ca. 1 nm). Figure 2 is a dynamic light scattering (DLS) pattern, which shows that the average hydrodynamic diameter of lactobionic acid coated ultra-small $Gd_2O_3$@MnO nanoparticles is 4.6 nm, which is larger than the average particle diameter observed in both HVEM and STEM images.

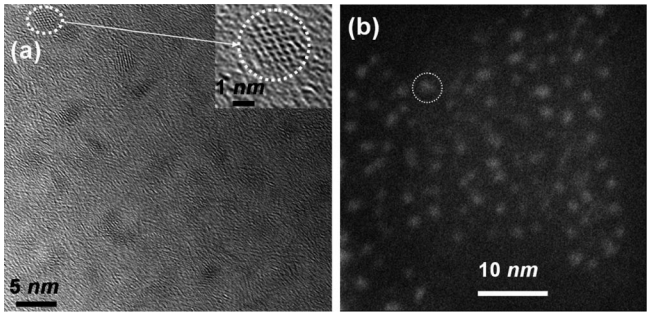


Figure 1. (a) HVEM and (b) STEM micrographs of lactobionic acid coated ultra-small $Gd_2O_3$@MnO nanoparticles. Dotted circles in both (a) and (b) indicate a single nanoparticle.

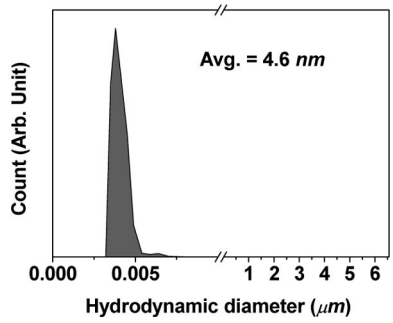


Figure 2. A DLS pattern of the lactobionic acid coated ultra-small $Gd_2O_3$@MnO nanoparticles.

### 2. Surface Coating

Surface coating by lactobionic acid was confirmed from the FTIR absorption spectrum of a powder sample (Figure 3). Stretches of the functional groups of lactobionic acid such as the C=O at 1600 $cm^{-1}$, C–H at 2910 $cm^{-1}$, and C–O at approximately 1080 $cm^{-1}$ in the FTIR absorption spectrum confirmed the surface coating. It is known that carboxylic acids chemically bind to surface metal ions.[8,24–27] This can be inferred from the redshifted C=O stretch. In this case, the C=O stretch is redshifted by approximately 110 $cm^{-1}$ from about 1710 $cm^{-1}$ for a free lactobionic acid, which is consistent with $Gd_2O_3$ nanoparticles coated by various carboxylic acids.[8] A strong peak at 1710 $cm^{-1}$ indicates that free lactobionic acids are not completely washed from the sample. The mass percentage of

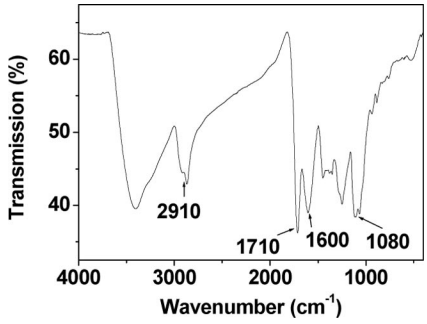


Figure 3. FTIR absorption spectrum of lactobionic acid coated ultra-small $Gd_2O_3$@MnO nanoparticles.

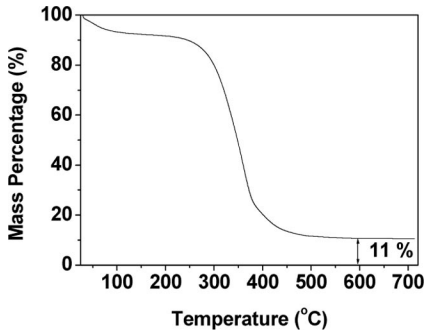


Figure 4. TGA curve of lactobionic acid coated ultra-small $Gd_2O_3$@MnO nanoparticles.

  

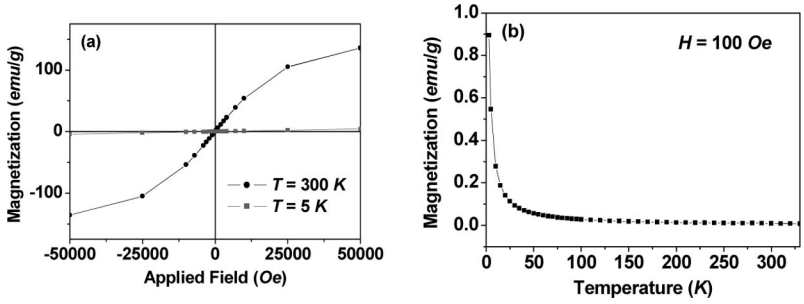


Figure 5. (a) Mass-corrected $M - H$ curves at 5 and 300 K and (b) mass-corrected ZFC $M - T$ curve at $H = 100$ Oe of lactobionic acid coated ultra-small $Gd_2O_3$@MnO nanoparticles.

ultra-small $Gd_2O_3$@MnO nanoparticles in lactobionic acid coated ultra-small $Gd_2O_3$@MnO nanoparticles was estimated to be approximately 11% by recording a thermogravimetric analysis (TGA) curve (Figure 4). This mass percentage was used to estimate the net magnetization of the ultra-small $Gd_2O_3$@MnO nanoparticles in lactobionic acid coated ultra-small $Gd_2O_3$@MnO nanoparticles.

## 3. Magnetic Properties

The magnetic properties were characterized by recording $M - H$ curves at 5 and 300 K (Figure 5a) and a zero-field-cooled (ZFC) $M - T$ curve at an applied field of 100 Oe (Figure 5b). Magnetizations in both $M - H$ and $M - T$ curves were mass-corrected to obtain the net magnetizations by using the TGA result as mentioned above. The $M - H$ curves at 5 and 300 K show that both coercivity and remanence are zero (i.e. no hysteresis). This lack of hysteresis as well as the lack of magnetic transition down to 3 K in the ZFC $M - T$ curve shows that ultra-small $Gd_2O_3$@MnO nanoparticles are paramagnetic down to 3 K. Thus, it is expected that ultra-small $Gd_2O_3$@MnO nanoparticles can efficiently induce longitudinal relaxation of water protons. In fact, a high $r_1$ value was observed. From the $M - H$ curve at 5 K, the magnetic moment of the ultra-small $Gd_2O_3$@MnO nanoparticles was measured to be 136 emu $g^{-1}$ at an applied field of 5 T. This value is smaller than that of 212 emu $g^{-1}$ for $Gd_2O_3$.[28] This is likely to be due two factors, firstly the MnO surface doping and secondly because the $M - H$ curve is not fully saturated at 5 T.

## 4. In-Vitro Map Images and Relaxivities

In order to test the MRI contrasting capability of an aqueous solution of the lactobionic acid coated ultra-small $Gd_2O_3$@MnO nanoparticles in vitro, dose-dependent $T_1$ and $T_2$ map images were measured (Figure 6a and b, respectively). They show clear dose-dependent contrast enhancements, which are due to the increased relaxation of water protons with increased dose. This shows the potential of lactobionic acid coated ultra-small $Gd_2O_3$@MnO nanoparticles as both $T_1$ and $T_2$ MRI contrast agents. The longitudinal ($T_1$) and transverse ($T_2$) relaxation times were also measured at various $Gd^{III}$ ion concentrations. The $r_1$ and $r_2$ values were then estimated to be 12.8 and 26.6 $s^{-1}$ $mM^{-1}$ from the slopes of the $1/T_1$ (= $r_1$) and $1/T_2$ (= $r_2$) plots vs. the $Gd^{III}$ ion concentration, respectively (Figure 7). Compared to ultra-small $Gd_2O_3$ nanoparticles,[8–15] the $r_1$ value is similar but the $r_2$ value is nearly double due to the MnO surface-doping as discussed below.

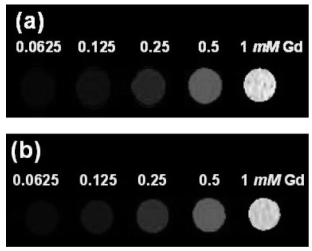


Figure 6. (a) In vitro $T_1$ and (b) $T_2$ map images of the sample solution, clearly showing contrast enhancements in both $T_1$ and $T_2$ map images with increasing dose.

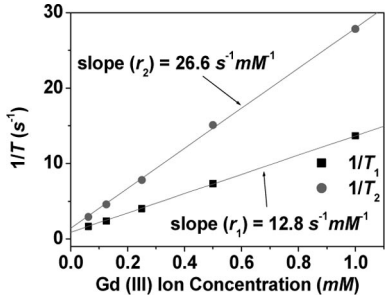


Figure 7. Plots of inverse relaxation times vs. $Gd^{III}$ ion concentration of the sample solution (the slopes correspond to relaxivities).

The Mn/Gd molar ratio of the sample was estimated to be approximately 0.11:1 with an inductively coupled plasma atomic emission spectrometer (ICPAES), showing that the nanoparticles are the MnO surface-doped $Gd_2O_3$ nanoparticles rather than the core-shell nanoparticles, because the Mn concentration is low. The measured $r_1$ and $r_2$ values confirmed this. That is, the measured $r_1$ value is similar to that of ultra-small $Gd_2O_3$ nanoparticles, but the measured $r_2$ value is nearly double that of the ultra-small $Gd_2O_3$ nanoparticles, as mentioned before. This is likely to be, because $r_1$ and $r_2$ are determined by the material with a higher relaxivity. $Gd^{III}$ ions close to the nanoparticle surface mainly contribute to $r_1$, whereas the surface-doped MnO

  

mainly contributes to $r_2$, because $r_1(Gd_2O_3) > r_1(MnO)$[29] and $r_2(Gd_2O_3) < r_2(MnO)$. This shows that $r_2$ can be improved by doping with a metal oxide with a high $r_2$ value at the same time as keeping the $r_1$ value of the ultra-small $Gd_2O_3$ nanoparticles. The values measured for $r_1$ and $r_2$ as well as those of other chemicals are provided in Table 1. The $r_1$ value of the ultra-small $Gd_2O_3$@MnO nanoparticles is not the same as that of the ultra-small $Gd_2O_3$ nanoparticles, which is likely to be due to the particle-size effect.[15] Table 1 shows that the nanoparticles have higher $r_1$ and $r_2$ values than molecular $Gd^{III}$ chelates, clearly showing that nanoparticles can be a more sensitive MRI contrast agent.

Table 1. Relaxivities ($r_1$, $r_2$) and particle diameters ($d$) of various chemicals including lactobionic acid coated ultra-small $Gd_2O_3$@MnO nanoparticles.

| Chemical | Ligand | $d$ | $r_1$ | $r_2$ | $r_2/r_1$ | Ref. |
|---|---|---|---|---|---|---|
| $Gd^{III}H_2O$ | DTPA[a] | – | 4.1 | 4.5 | 1.1 | [30] |
| $Gd_2O_3$ | D-glucuronic acid | 1.0 | 9.9 | 10.9 | 1.1 | [15] |
| $Gd_2O_3$@MnO | lactobionic acid | 1.5 | 12.8 | 26.6 | 2.1 | this work |
| MnO | lactobionic acid | 1.9 | 6.9 | 67.7 | 9.8 | [29] |

[a] Diethylenetriaminepentaacetic acid.

### 5. In-Vivo Test

To further investigate the $T_1$ MRI contrasting capability, we tested the sample solution in vivo by taking 3 T $T_1$ MR images of a mouse. Before we carried out this measurement, we performed an in-vitro cytotoxicity test of the sample solution by using two different cell lines up to 5 μM of $Gd^{III}$ ion concentration (Figure 8). This test shows that lactobionic acid coated ultra-small $Gd_2O_3$@MnO nanoparticles are not toxic in the concentration range studied. The MR images obtained are shown in Figure 9. A slight contrast enhancement in all parts can be seen 90 min after injection of the sample solution. These in-vivo $T_1$ MR images show a high contrast enhancement in kidneys, likely due to excretion of nanoparticles from the organs through the kidneys, which is an important requirement for MRI contrast agents, because the nanoparticles should eventually be excreted by the kidneys.

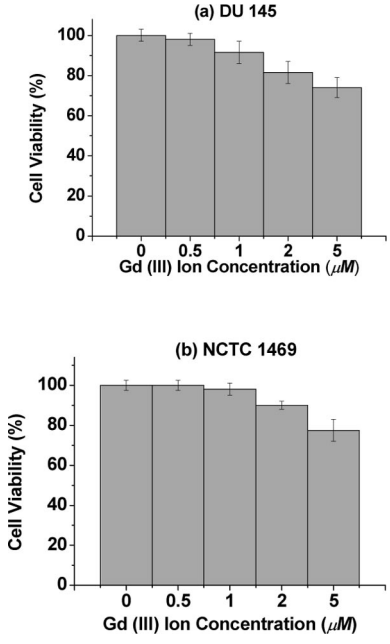


Figure 8. Cytotoxicity tests of the sample solution by using (a) DU 145 and (b) NCTC 1469 cell lines.

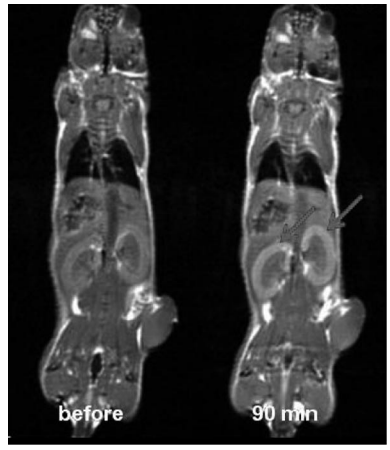


Figure 9. 3 T in-vivo $T_1$ MR images of a mouse before (left) and 90 min after (right) injection of the sample solution into the tail vein of the mouse, showing a clear contrast enhancement in the kidneys (shown by arrows).

## Conclusions

We synthesized ultra-small $Gd_2O_3$ nanoparticles, which were surface-doped by MnO by first synthesizing the ultra-small $Gd_2O_3$ nanoparticles and then subsequently coating (or doping) them with MnO. The Mn/Gd mmol ratio in the ultra-small $Gd_2O_3$@MnO nanoparticles was approximately 0.11:1. They were further coated with hydrophilic biocompatible lactobionic acid. The surface-doped nanoparticles ranged from 1 to 2 nm in diameter. The $r_1$ and $r_2$ values were estimated to be 12.8 and 26.6 $s^{-1}mM^{-1}$, respectively. Compared to the ultra-small $Gd_2O_3$ nanoparticles, $r_1$ was nearly the same, whereas $r_2$ was nearly double due to the MnO surface doping. This shows that $r_2$ can be improved by doping with metal oxides with high $r_2$ values on ultra-small $Gd_2O_3$ nanoparticles while retaining the $r_1$ relaxivity of the ultra-small $Gd_2O_3$ nanoparticles. In-vitro tests of the sample solution showed clear dose-dependent contrast enhancements in both $T_1$ and $T_2$ map images. The performance of the sample solution as a $T_1$ MRI contrast agent was proved in vivo with $T_1$ MR images of a mouse. The sample solution certainly provides better $T_2$ MR images than the undoped ultra-small $Gd_2O_3$ nanoparticles although their capability as a $T_2$ MRI contrast agent will be less than that of SPIO.

## Experimental Section

In order to synthesize lactobionic acid coated ultra-small $Gd_2O_3$@MnO nanoparticles, ultra-small $Gd_2O_3$ nanoparticles were

  

first synthesized and then surface-doped with MnO. Finally, lactobionic acid was coated on the ultra-small $Gd_2O_3$@MnO nanoparticles. $GdCl_3 \cdot xH_2O$ (5 mmol) was added to triethylene glycol (40 mL) and the mixture heated to reflux at 250 °C for 24 h with magnetic stirring and air bubbling. After it had cooled to 100 °C, $MnCl_2 \cdot 4H_2O$ (5 mmol) was added to the reaction solution. The reaction solution was heated to reflux at 250 °C for a further 24 h with magnetic stirring and air bubbling. After cooling to 150 °C, lactobionic acid (5 mmol) was added to the reaction solution, which was magnetically stirred at that temperature for another 24 h. After cooling to room temperature, unreacted $Gd^{III}$, $Cl^-$ ions, and solvent were removed from the reaction solution by repeating the following procedure three times: firstly, the reaction solution was diluted with distilled water (500 mL) and then allowed to stand for a week until most of the nanoparticles had settled to the bottom. Secondly, the top part of the solution was decanted. After washing, the remaining solution was centrifuged (4000 rpm, 1 h). The precipitated nanoparticles were then collected. Half of the yielded nanoparticles were redispersed in distilled water for relaxivity and MR image measurements, and the remainder was dried in air to obtain a powder sample for the other characterizations. All chemicals were purchased from Aldrich and used as received. HVEM (JEOL JEM-ARM 1300S, 1.2 MeV acceleration voltage) and STEM (JEOL, JEM 2100F, 200 kV acceleration voltage) were used to measure particle diameters of the lactobionic acid coated ultra-small $Gd_2O_3$@MnO nanoparticles. The difference was used to estimate the thickness of the surface coating by lactobionic acid. The nanoparticles were dispersed in methanol (99.999%) and loaded onto a copper grid covered with an amorphous carbon membrane. A DLS particle-size analyzer (UPA-150, Microtrac) was used to measure the hydrodynamic diameter of the lactobionic acid coated ultra-small $Gd_2O_3$@MnO nanoparticles. The doping amount of MnO was determined in terms of Mn/Gd molar ratio by using ICPAES (Thermo Jarrell Ash Co., IRIS/AP). Nanoparticles in a 1.0 g sample solution were completely dissolved by treating the sample solution with 4 mL of HCl (or 3 mL HCl and 1 mL $HClO_4$) and heated at 50–60 °C until the nanoparticles were completely dissolved in the solution. 2–3% $HNO_3$ solution was added to dilute the sample solution. The total weight of the final solution was measured and the solution was then used for the ICPAES measurement. A superconducting quantum interference device magnetometer (Quantum Design, MPMS-7) was used to characterize the magnetic properties of the ultra-small $Gd_2O_3$@MnO nanoparticles by recording both $M - H$ curves at 5 and 300 K and a ZFC $M - T$ curve at an applied field of 100 Oe. In order to measure these curves, an exact mass (10–20 mg) of the powder sample was loaded into a nonmagnetic capsule. In order to obtain a net magnetization measurement of the ultra-small $Gd_2O_3$@MnO nanoparticles, correction of the sample mass was made by recording a TGA (TA Instruments, SDT Q 600) curve because the ultra-small $Gd_2O_3$@MnO nanoparticles were coated with lactobionic acid. The TGA curve was scanned between room temperature and 700 °C under a flow of air. An FTIR absorption spectrometer (Mattson Instruments, Inc., Galaxy 7020A) was used to characterize the surface coating by lactobionic acid. To record an FTIR absorption spectrum (400–4000 $cm^{-1}$), a pellet was prepared by pressing a mixture of the powder sample with KBr. Both $T_1$ and $T_2$ map images as well as both $T_1$ and $T_2$ relaxation times were measured with an MRI instrument (GE 1.5 T, Excite) equipped with the Knee coil (EXTREM). A $Gd^{III}$ ion concentration of an original sample solution was measured with ICPAES. Then, five aqueous solutions of different $Gd^{III}$ ion concentrations (1, 0.5, 0.25, 0.125, 0.0625 mM) were prepared by diluting the original sample solution with distilled water and used for both relaxivity and map image measurements. The experimental conditions for these measurements have been described in detail previously.[31] The in-vitro cytotoxicity test of the sample solution was performed by using both human prostate cancer (DU145) and normal mouse hepatocyte cell lines (NCTC1469) for $Gd^{III}$ ion concentrations up to 5 μM. Each cell viability test was normalized with respect to the corresponding control cell lines with 0.0 M $Gd^{III}$ ion concentration. The cellular toxicity was quantified by measuring the intracellular ATP by using the CellTiter-Glo Luminescant Cell Viability Assay (Promega) and a luminometer (Victor 3, Perkin–Elmer). Cells were seeded on a 24-well cell-culture plate at the density of $5 \times 10^4$ with 500 μL volume per well, and they were incubated for 24 h (5% $CO_2$, 37 °C). Approximately 2 μL of various concentrations (0–5 μM Gd) of the contrast agent prepared in a sterile phosphate-buffered saline (PBS) solution, were introduced into the cell culture media and incubated for 48 h before the cell viability test. The in-vivo $T_1$ MR-image study was performed in accordance with the rules of the animal research committee of the Kyungpook National University. Six-week male ICR mice with weights of 29–31 g were used for the in-vivo study. The mice ($n$ = 6) were anesthetized by 1.5% isoflurane in oxygen. Measurements were made before and after injection of the sample solution (0.07 mmol Gd/kg) through the tail vein. After each measurement, the mouse was revived from anesthesia, and placed in the cage with free access to food and water. During the measurements, the mice were maintained at approximately 37 °C by using a warm water blanket. MR images were taken with a 3.0 T MR unit (GE Healthcare) equipped with a home-made small animal RF coil. The coil was of the receiver type with an inner diameter of 50 mm. The imaging parameters for $T_1$ 3D fast SPGR (spoiled GRASS images) are as follows: repetition time = 9.2 ms; echo time = 2.1 ms; 12 mm field of view; $256 \times 192$ matrix size; 0.8 mm slice thickness; number of acquisitions = 8.

## Acknowledgments

This work was supported by the Regional Technology Innovation Program of the Ministry of Commerce, Industry, and Energy funded by the Korean Government (grant No. RTI04-01-01), the Basic Science Research Program through the National Research Foundation (NRF) funded by the Ministry of Education, Science and Technology (2010-0002436), and the Ministry for Health, Welfare & Family Affairs, ROK through the Korea Healthcare technology R&D Project (grant No. A090193). We thank the Korea Basic Science Institute for allowing us to use their HVEM.

[1] Q. A. Pankhurst, N. K. T. Thanh, S. K. Jones, J. Dobson, *J. Phys. D: Appl. Phys.* **2009**, *42*, 224001.
[2] A. G. Roca, R. Costo, A. F. Rebolledo, S. Veintemillas-Verdaguer, P. Taraj, T. González-Carreño, M. P. Morales, C. J. Serna, *J. Phys. D: Appl. Phys.* **2009**, *42*, 224002.
[3] C. W. Jung, *Magn. Reson. Imaging* **1995**, *13*, 675–691.
[4] C. W. Jung, P. Jacobs, *Magn. Reson. Imaging* **1995**, *13*, 661–674.
[5] E. V. Groman, L. Josephson, J. M. Lewis, *U. S. Patent* 4827945, **1989**.
[6] S. Palmacci, L. Josephson, *U. S. Patent* 5262176, **1993**.
[7] H. B. Na, J. H. Lee, K. An, Y. I. Park, M. Park, I. S. Lee, D.-H. Nam, S. T. Kim, S.-H. Kim, S.-W. Kim, K.-H. Lim, K.-S. Kim, S.-O. Kim, T. Hyeon, *Angew. Chem. Int. Ed.* **2007**, *46*, 5397–5401.
[8] F. Söderlind, H. Pedersen, R. M. Petoral, P.-O. Käll, K. Uvdal, *J. Colloid Interface Sci.* **2005**, *288*, 140–148.
[9] M. Engström, A. Klasson, H. Pedersen, C. Vahlberg, P.-O. Käll, K. Uvdal, *Magn. Reson. Mater. Phys.* **2006**, *19*, 180–186.

  

[10] M.-A. Fortin, R. M. Petoral, F. Söderlind, A. Klasson, M. Engström, T. Veres, P.-O. Käll, K. Uvdal, *Nanotechnology* **2007**, *18*, 395501.
[11] R. Bazzi, M. A. Flores, C. Louis, K. Lebbou, W. Zhang, C. Dujardin, S. Roux, B. Mercier, G. Ledoux, E. Bernstein, P. Perriat, O. Tillement, *J. Colloid Interface Sci.* **2004**, *273*, 191–197.
[12] R. M. Petoral, F. Söderlind, A. Klasson, A. Suska, M. A. Fortin, N. Abrikossova, L. Selegård, P.-O. Käll, M. Engström, K. Uvdal, *J. Phys. Chem. C* **2009**, *113*, 6913–6920.
[13] J.-L. Bridot, A.-C. Faure, S. Laurent, C. Rivière, C. Billotey, B. Hiba, M. Janier, V. Josserand, J.-L. Coll, L. V. Elst, R. Muller, S. Roux, P. Perriat, O. Tillement, *J. Am. Chem. Soc.* **2007**, *129*, 5076–5084.
[14] J. Miyawaki, M. Yudasaka, H. Imai, H. Yorimitsu, H. Isobe, E. Nakamura, S. Lijima, *J. Phys. Chem. B* **2006**, *110*, 5179–5181.
[15] J. Y. Park, M. J. Baek, E. S. Choi, S. Woo, J. H. Kim, T. J. Kim, J. C. Jung, K. S. Chae, Y. Chang, G. H. Lee, *ACS Nano* **2009**, *3*, 3663–3669.
[16] H. Hifumi, S. Yamaoka, A. Tanimoto, D. Citterio, K. Suzuki, *J. Am. Chem. Soc.* **2006**, *128*, 15090–15091.
[17] F. Evanics, P. R. Diamente, F. C. J. M. van Veggel, G. J. Stanisz, R. S. Prosser, *Chem. Mater.* **2006**, *18*, 2499–2505.
[18] W. J. Rieter, K. M. L. Taylor, H. An, W. Lin, W. Lin, *J. Am. Chem. Soc.* **2006**, *128*, 9024–9025.
[19] a) I.-F. Li, C.-H. Su, H.-S. Sheu, H.-C. Chiu, Y.-W. Lo, W.-T. Lin, J.-H. Chen, C.-S. Yeh, *Adv. Funct. Mater.* **2008**, *18*, 766–776; b) K.-W. Hu, F.-Y. Jhang, C.-H. Su, C.-S. Yeh, *J. Mater. Chem.* **2009**, *19*, 2147–2153.
[20] I.-F. Li, C.-S. Yeh, *J. Mater. Chem.* **2010**, *20*, 2079–2081.
[21] P. Caravan, J. J. Ellison, T. J. McMurry, R. B. Lauffer, *Chem. Rev.* **1999**, *99*, 2293–2352.
[22] L. Banci, I. Bertini, C. Luchinat, *Nuclear and Electron Relaxation*, VCH, Weinheim, **1991**.
[23] a) G. J. Strijkers, W. J. M. Mulder, G. A. F. van Tilborg, K. Nicolay, *Anti-Cancer Agents Med. Chem.* **2007**, *7*, 291–305; b) A. C. Silva, J. H. Lee, I. Aoki, A. P. Koretsky, *NMR Biomed.* **2004**, *17*, 532–543; c) J. Crossgrove, W. Zheng, *NMR Biomed.* **2004**, *17*, 544–553; d) M. R. Goldman, T. J. Brady, I. L. Pykett, C. T. Burt, F. S. Buonanno, J. P. Kistler, J. H. Newhouse, W. S. Hinshaw, G. M. Pohost, *Circulation* **1982**, *66*, 1012–1016.
[24] C. B. Mendive, T. Bredow, M. A. Blesa, D. W. Bahnemann, *Phys. Chem. Chem. Phys.* **2006**, *8*, 3232–3247.
[25] S. J. Hug, D. Bahnemann, *J. Electron Spectrosc. Relat. Phenom.* **2006**, *150*, 208–219.
[26] O. W. Duckworth, S. C. Martin, *Geochim. Cosmochim. Acta* **2001**, *65*, 4289–4301.
[27] A. D. Roddick-Lanzilotta, A. J. McQuillan, *J. Colloid Interface Sci.* **1999**, *217*, 194–202.
[28] C. J. Schinkel, W. D. Van Amstel, *Phys. Lett. A* **1973**, *44*, 467–468.
[29] J. Y. Park, E. S. Choi, M. J. Baek, G. H. Lee, S. Woo, Y. Chang, *Eur. J. Inorg. Chem.* **2009**, *17*, 2477–2481.
[30] R. B. Lauffer, *Chem. Rev.* **1987**, *87*, 901–927.
[31] J. Y. Park, P. Daksha, G. H. Lee, S. Woo, Y. Chang, *Nanotechnology* **2008**, *19*, 365603.

Received: April 3, 2010
Published Online: August 5, 2010

  